Aberrant frontostriatal connectivity in Alzheimer's disease with positive palmomental reflex

H. Gramespacher[a] (iD), N. Richter[a,b], S. Edwin Thanarajah[a,c,d], H. I. L. Jacobs[e,f], K. N. H. Dillen[b,g], N. Nellessen[a], B. von Reutern[a,b], J. Dronse[a,b], J. Kukolja[a,h,i], G. R. Fink[a,b] and O. A. Onur[a,b] (iD)

[a]Department of Neurology, Faculty of Medicine and University Hospital Cologne, University of Cologne, Cologne; [b]Cognitive Neuroscience, Research Center Jülich, Institute of Neuroscience and Medicine (INM3), Research Centre Juelich, Juelich; [c]Max Planck Institute for Metabolism Research, Cologne; [d]Department of Psychiatry, Psychosomatic Medicine and Psychotherapy, University Hospital Frankfurt, Frankfurt, Germany; [e]Faculty of Health, Medicine and Life Sciences, School for Mental Health and Neuroscience, Alzheimer Centre Limburg; Maastricht University, Maastricht, The Netherlands; [f]Gordon Center of Medical Imaging, Department of Radiology, Massachusetts General Hospital, Harvard Medical School, Boston, MA, USA; [g]Department of Palliative Medicine, Faculty of Medicine and University Hospital Cologne, University of Cologne, Cologne; [h]Department of Neurology and Clinical Neurophysiology, Helios University Hospital Wuppertal, Wuppertal; and [i]Faculty of Health, Witten/Herdecke University, Witten, Germany

Background and purpose: Primitive reflexes may reoccur in various neurodegenerative diseases. However, little is known about their structural and functional correlates in the human brain. Notably, the neural mechanisms underlying a positive palmomental reflex (PMR) are poorly understood. As recent studies link Alzheimer's disease (AD)-related primitive reflexes to a dysfunction of the corticostriatal motor circuit (CMC), we conducted the present study to investigate functional and structural correlates of a positive PMR. We hypothesized an involvement of frontostriatal structures and an impairment of the CMC.

Methods: Using whole-brain resting-state functional connectivity (FC), hypothesis and FC result-based probabilistic tractography, and voxel-based morphometry analyses, we compared two groups of AD patients with either positive ($n = 12$) or negative PMR ($n = 12$).

Results: No significant differences in grey matter volume or structural connectivity (SC) could be observed between the PMR-positive and PMR-negative groups. In contrast, the PMR-positive group showed a decreased seed-to-voxel FC between the bilateral supplementary motor area and parts of the right-hemispherical caudate nucleus and thalamus and a decreased region of interest (ROI)-to-ROI FC between the left putamen and the left superior frontal gyrus.

Conclusion: Data suggest that dysfunction of the CMC reflected by decreased FC underlies a positive PMR in patients with AD. The lack of significant grey matter or SC differences might reflect that changes in FC appear before changes in SC in the structures of the CMC and brain atrophy.

Introduction

Diagnosing Alzheimer's disease (AD) is a complex, multi-level process using, amongst other factors, the patient's history, neurological and neuropsychological assessment, neuroimaging, cerebrospinal fluid (CSF)-based biomarkers, and neuropathology [1]. While combinations of these procedures can detect AD with high sensitivity and specificity, clear signs in the clinical examination are lacking. One (albeit unspecific) clinical sign often attributed to AD is the palmomental reflex (PMR) [2]. Although some authors consider a positive

Correspondence: H. Gramespacher, Department of Neurology, Faculty of Medicine and University Hospital Cologne, University of Cologne, Cologne, Germany (tel.: +49-(0)221-47886067; fax: +49-(0)221-47886068; e-mail: hannes.gramespacher@uk-koeln.de).

PMR as helpful in patients suspected of having dementia [3], its functional and neural underpinnings in neurodegeneration remain by and large unknown.

The PMR is a polysynaptic reflex that, triggered by nociceptive stimulation of the thenar eminence, leads to a mostly ipsilateral involuntary contraction of the mentalis muscle [4,5]. The PMR is physiological in infants up to an age of approximately 12 months and then disappears, presumably due to the maturation of the frontal lobes. Therefore, its reappearance in elderly individuals and patients with frontal pathology is considered as a 'frontal lobe sign' or 'cortical release sign', assuming a lack of frontal inhibition exerted on subcortical motor networks [5,6]. Indeed, although the PMR can be detected in people of all ages and states of health [7,8], a positive PMR occurs more frequently in neurological conditions, for example, stroke, multiple sclerosis, motor neurone disease, and dementia [7]. Furthermore, the PMR has been associated with basal ganglia dysfunction [9], in particular, Parkinson's disease [10].

Consistently, recent studies link an AD-related PMR to corticostriatal dysfunction [11], suggesting, on the one hand, an involvement of the motor circuit via interconnecting axonal loops between the prefrontal, premotor [including the supplementary motor area (SMA)], and motor cortex, and, on the other hand, the basal ganglia, thalamus and cerebellum [12]. The aim of the present study was to investigate structural and functional correlates of a positive PMR in patients with AD, with particular emphasis on the frontostriatal networks. We hypothesized that a positive PMR in AD patients would be associated with impaired connectivity of the corticostriatal motor circuit (CMC). To test these hypotheses, we compared two groups of biomarker-positive AD with either a positive or negative PMR, assessing functional connectivity (FC), diffusion tensor imaging-based probabilistic tractography as a measure of structural connectivity (SC), and voxel-based morphometry.

Methods

Participants

Patients were selected from the COPCAD (SC and FC alterations in the posterior cingulate cortex in Alzheimer's disease) study [13] conducted by the Department of Neurology, University Hospital Cologne, University of Cologne, in cooperation with the Institute Neuroscience and Medicine - Cognitive Neuroscience (INM-3), Research Centre Jülich.

Alzheimer's disease was diagnosed by an interdisciplinary team of clinicians with extensive experience in dementia care and research. Patients had to show the typical clinical syndrome according to the guidelines proposed by the National Institute on Aging-Alzheimer's Association (NIA-AA) [14], which state that the patient should show subtle onset and slow progression of cognitive impairment (either self-reported or reported by a third party), and memory deficits with a standard deviation of >1.5 below average in any of the neuropsychological testing results (adjusted for age, sex, and education).

In addition, the diagnosis was supported by the A/T/N biomarker classification system [15], mainly considering CSF biomarkers and applying the cutoff values proposed by Mulder *et al.* [16]. 'A' refers to confirmed amyloid pathology (CSF amyloid-beta-1-42 < 550 pg/ml), 'T' refers to the value of phosphorylated tau protein (pTAU > 52 pg/ml) and 'N' represents signs of neurodegeneration or neuronal injury (CSF total tau > 375 pg/ml). Only patients who met clinical criteria for AD dementia and probable AD according to the A/T/N biomarker classification system were included.

Twelve patients were excluded from the present analysis because of a non-AD CSF biomarker profile ($n = 8$) or a psychiatric disorder, e.g. major depression ($n = 4$). The patients fulfilling all the inclusion criteria were divided into two groups, consisting of 12 patients each, depending on whether the PMR was positive or negative.

The PMR-positive group ranged between 55 and 75 years of age [mean (SD) age 69.75 (5.96) years] and included seven women. The PMR-negative group ranged between 59 and 78 years of age [mean (SD) age 69.08 (7.37) years] and included four women.

Statistical analyses of demographic, neuropsychological and non-cognitive data were performed using SPSS software (Version 24; SPSS Inc., Chicago, IL, USA). To examine group differences, a Mann−Whitney U-test was conducted, respecting the central limit theorem defining significance at $P < 0.05$. Furthermore, the neuropsychological data were correlated with our main finding FC values, computing Spearman's correlations as a measure of the (bivariate) linear correlation defining significance at $P < 0.05$ (two-sided).

The study was approved by the local ethics committee and followed the Declaration of Helsinki. Written informed consent was provided by all patients.

Palmomental reflex

To test the PMR, the examiner stroked the thenar eminence in a proximal to distal direction and the PMR was considered positive when a distinct brief contraction of the ipsilateral mentalis muscle was observed. The PMR was exclusively assessed by

experienced and trained neurologists of the Department of Neurology, University Hospital Cologne.

Neuropsychological testing

Each patient underwent a comprehensive neuropsychological assessment, covering several cognitive domains, including memory, attention, visuospatial abilities, language, executive functions, and sensorimotor skills.

Neuropsychological testing was performed within the scope of the COPCAD study as described by Dillen et al. [17].

Magnetic resonance imaging data acquisition

Resting-state functional, anatomical and diffusion tensor imaging was performed using a 3T whole-body magnetic resonance imaging (MRI) system (Siemens MAGNETOM Trio System, Erlangen, Germany) equipped with a 32-channel head coil. The parallel imaging scheme GRAPPA (GeneRalized Autocalibrating Partially Parallel Acquisitions) and an acceleration factor of two were applied. During the 7-min resting-state functional MRI, patients were instructed to remain still and keep their eyes open in order to avoid falling asleep. A T2*-weighted, single-shot echo planar imaging sequence with blood oxygen level-dependent (BOLD) contrast was acquired with the following parameters: repetition time $=3000$ ms, echo time $=30$ ms, flip angle $=90°$, field of view $=200 \times 200$ mm^2, matrix $=80 \times 80$, voxel-resolution $=2.5 \times 2.5 \times 2.9$, gap $=0.28$ mm. High-resolution, T1-weighted, three-dimensional anatomical images were collected using a 3DMPRAGE (Magnetization Prepared Rapid Acquisition Gradient-Echo) sequence with repetition time $=2250$ ms, echo time $=3.03$ ms, flip angle $=9°$. This sequence consisted of 176 sagittal slices of 1-mm^3 isotropic voxels with an in-plane matrix of 256×256.

Diffusion tensor imaging was performed using a single-shot diffusion-weighted echo planar imaging sequence with the following specifications: repetition time $=8900$ ms, echo time $=116$ ms, slice thickness $=2.5$ mm, voxel-size $=2.5$ mm, field of view $=240$ mm, 150 different directions, number of averages $=1$, multi-shell diffusion acquisition with multiple b-values (10 $b = 0$ s/mm^2, $b = 700$ s/mm^2, $b = 1000$ s/mm^2 and $b = 2800$ s/mm^2), acquiring 60 transversal slices.

Functional connectivity analysis

The preprocessing and FC analyses were performed using the FC toolbox CONN v.15.h [18], based on MATLAB (MATLAB R2016a; MathWorks Inc., Natick, MA, USA, 2000) and the Statistic Parametric Mapping software (SPM12, Wellcome Department of Imaging Neuroscience, London, UK, http://www.fil.ion.ucl.ac.uk). The first four images of the resting-state data were removed to ensure a steady-state equilibrium. High-resolution structural data and resting-state functional data were preprocessed using the preprocessing pipeline implemented in CONN and based on SPM12, which included functional realignment and unwarping, slice-time correction, structural segmentation and normalization to Montreal Neurological Institute (MNI) space, functional normalization to MNI space, outlier detection, and smoothing with a Gaussian smoothing kernel specified at 8 mm FWHM (full width at half maximum).

For our analysis, we used the pre-defined regions of interest (ROIs) provided by CONN, based on the Harvard-Oxford atlas of cortical and subcortical areas [19].

First-level covariates regarding within-subject effects were derived from the realignment (six rigid-body parameters characterizing the estimated subject motion for each subject and session) and the artifact detection tools-based scrubbing parameters.

Afterwards, a denoising step was applied in order to define, explore, and remove confounding effects, such as motion and other noise sources, from the BOLD signal. White matter and CSF BOLD time series were regressed out using a component-based method to reduce noise (CompCor), as well as the first-level covariates (motion and scrubbing parameters).

Fisher-transformed bivariate correlation coefficients were computed between each of the 132 pre-defined ROI BOLD time series (averaged across all ROI voxels) provided by CONN and each individual voxel BOLD time series (seed-to-voxel analysis) in order to identify whole-brain, voxel-wise connectivity maps of areas showing correlated activity with one or more seeds. Given the a priori hypothesis and according to our seed-to-voxel FC results, ROI-to-ROI FC matrices (again using Fisher-transformed bivariate correlation coefficients between ROI BOLD time series averaged across all ROI voxels) were computed, focusing on the ROIs being part of the frontostriatal motor circuit (i.e. the prefrontal cortex, premotor cortex, primary motor cortex, thalamus, and basal ganglia) to compute ROI-to-ROI connectivity values for each subject.

Group differences between PMR-positive and PMR-negative patients were assessed using a two-sample t-test. The general linear model was applied for all second-level analyses of FC data.

The seed-to-voxel second-level analysis results were thresholded using a peak-voxel family-wise error (FWE)-corrected threshold of $P < 0.005$ (two-sided). The ROI-to-ROI analysis was thresholded using a one-sided false discovery rate (FDR)-corrected P-value of $P < 0.05$ to detect subtle between-group effects.

Tractography

Diffusion-weighted images were analysed using FMRIB's (Oxford Centre for Functional MRI of the Brain) diffusion toolbox (FDT) in FMRIB's Software Library (FSL, FMRIB Software Library Version 5.0, University of Oxford, 2012, http://fsl.fmrib.ox.ac.uk/fsl/fslwiki/FSL [20]).

After converting the diffusion-weighted Digital Imaging and Communications in Medicine (DICOM) images to four-dimensional Neuroimaging Informatics Technology Initiative (NIfTI) data format and generating the b-values (bvals) and gradient directions (bvecs) using the dcm2nii toolbox [21], we created a brain mask of each patient. T1 images were segmented using SPM12, as the output of FSL's Brain Extraction Toolbox BET [22] was flawed in some cases. The resulting grey and white matter masks were combined, binarized, reoriented to standard space, coregistered to the diffusion images using FSL FLIRT [23], and used to mask out non-brain tissue from the diffusion images. Target and seed masks were created using masks of the SMA, superior frontal gyrus (SFG), putamen, caudate nucleus, and thalamus, as defined in the Wake Forest University Pickatlas Tool [24] with the Automated Anatomical Labeling Atlas [25]. In addition, we used clusters extracted from our FC seed-to-voxel analysis results to create FC result-based masks, which were subsequently resliced. Consequently, we received one mask, covering parts of the right caudate nucleus and the right thalamus (CE1), and a second mask, which was additionally multiplied with an atlas-based mask of the right caudate nucleus, thus containing only parts of the right caudate nucleus (CE2).

A preliminary data check was performed on the diffusion-weighted data and the brain masks considering the bvecs to check if the vectors were oriented adequately concerning the anatomy using FDT's DTIFIT tool. For correction of eddy current distortions and movements in diffusion data, we used FDT's eddy tool [26]. A revised fitting of diffusion tensors on our eddy-corrected data (again using DTIFIT) was followed by fitting of the probabilistic diffusion model on corrected data using FDT's BEDPOSTX tool, respecting the multi-shell model [27]. Non-linear FNIRT registration between structural space and the MNI 152 standard space was performed using the reoriented T1-weighted non-brain extracted structural data. The generated warps were combined with the coregistration parameters between diffusion and structural space and applied to the seed, target and exclusion masks to transform them into the individual's diffusion space for the analyses.

After these pre-processing steps, we ran a probabilistic diffusion tractography analysis using FDT's PROBTRACKX option [28] to reconstruct the fibre pathways between the masks. We defined our seeds and targets, as well as stop and waypoints (the last two constitute the target mask) following our main FC findings. We excluded the brainstem and cerebellum, as well as the contralateral hemisphere (as we were not interested in interhemispheric connections). FDT's PROBTRACKX was performed in diffusion space using the following parameters: the number of samples was 5000, step length was 0.5 mm, and the curvature threshold was 0.2. The analysis was conducted in both directions (A, B) and the number of fibre samples (K) from both directions corrected for the corresponding target mask size (N) and the number of total streamlines (5000) was averaged to estimate the structural connection probability (ϕ_{AB}) [29].

$$\phi_{AB} = \frac{\left(\frac{K_A}{N_A * 5000} + \frac{K_B}{N_B * 5000} \right)}{2}.$$

We performed visual quality control of the fibre tract images and masks using FSLView. Subsequently, an unpaired two-sample t-test was performed to detect possible group differences using SPSS software (Version 24; SPSS Inc.). Results were defined as significant at $P < 0.05$, Bonferroni-corrected for multiple comparisons (five comparisons).

Voxel-based morphometry

Voxel-based morphometry was performed to identify grey matter differences, based on a voxel-wise estimation of the local amount of grey matter.

The high-resolution T1-weighted MPRAGE sequences were preprocessed and analysed in MATLAB using the SPM12 framework with the provided default preprocessing pipeline for voxel-based morphometry analyses. The T1 volumes were segmented to extract the aligned grey and white matter images of every single subject. Afterwards, the DARTEL (Diffeomorphic Anatomical Registration Through Exponentiated Lie Algebra [30]) procedure was applied to estimate the non-linear deformations by alternating between creating a template and

registering the tissue classes with the template. Modulated and warped tissue class images were created using the flow field data to spatially normalize the native grey matter tissue class images to MNI space, including an affine registration of the DARTEL template to SPM's tissue probability map and a smoothing step with a Gaussian smoothing kernel specified at 8 mm FWHM. Statistical analysis was computed following the general linear model to detect grey matter differences between PMR-positive and PMR-negative patients. Model parameters were estimated using the restricted maximum likelihood algorithm. T-contrasts between groups were defined as significant at a FWE-corrected threshold of $P < 0.05$ and reported in MNI coordinates. Assigning output MNI coordinates to specific grey matter brain regions was conducted using the Automated Anatomical Labeling Atlas [25] in MRIcron (https://www.nitrc.org/projects/mricron).

Results

Demographic information, neuropsychological testing performance and biomarkers

No significant between-group differences in age, sex or education were observed. Furthermore, the two groups did not differ significantly in their neuropsychological performance and biomarkers (Table 1). Thus, none of these variables were considered as covariates.

Functional connectivity

Seed-to-voxel analysis
Whole-brain group comparisons (i.e. PMR-positive < PMR-negative) revealed reduced FC emerging from the left and right SMA in AD patients with a positive PMR compared to AD patients with a negative PMR.

The FC cluster emerging from the right SMA seed contained parts of the right caudate nucleus extending to the right thalamus. The FC cluster stemming from the left SMA seed also contained parts of the right caudate nucleus, likewise extending to the right thalamus (Fig. 1). No changes in FC were seen in the reverse seed-to-voxel FC analysis (i.e. PMR-negative < PMR-positive; Table 2).

ROI-to-ROI analysis
Group comparisons (i.e. PMR-positive < PMR-negative) revealed reduced ROI-to-ROI FC between the left putamen and the left SFG (T (22) = 3.96, P-uncorrected = 0.0003, P-FDR corrected = 0.0463) in the PMR-positive group compared to the PMR-negative

group. Reverse group effects (i.e. PMR-negative < PMR-positive) were not detected.

Correlation between functional connectivity and neuropsychological testing performance
Based on our main findings, we assessed whether the FC between the right and left SMA and the corresponding activation clusters covering parts of the right caudate nucleus and the right thalamus correlated with the cognitive performance of the patients as derived from neuropsychological testing. No significant correlations were detected.

Probabilistic tractography

No significant differences in structural connection strength between groups were detected.

Atlas- and FC result-based ROIs serving as seeds and targets in different settings were selected following our main FC findings (Table 3).

Voxel-based morphometry

No significant group differences in grey matter density were detected at the pre-determined level of significance (FWE-corrected $P < 0.05$). Decreasing the level of significance ($P < 0.001$, uncorrected, peak-level, extent threshold >10 voxels), PMR-negative patients showed higher grey matter volume in clusters in the left superior parietal lobule, right SFG and left middle temporal gyrus compared to the PMR-positive group. Reverse effects were not observed (Table 4).

Discussion

The present study aimed to identify the neural correlates of a reappeared PMR in AD, hypothesizing an involvement of frontostriatal structures and, through this, an impairment of the CMC.

The main finding of this study was a decreased seed-to-voxel FC between the SMA bilaterally and the right caudate nucleus and right thalamus in AD patients with a positive PMR (compared to AD patients with a negative PMR) in a whole-brain analysis.

The finding of impaired connectivity between structures belonging to the frontal lobe (SMA and SFG) and the neostriatum (caudate nucleus and putamen) is consistent with our hypothesis linking the PMR with a dysfunction in the CMC, which is composed of interconnecting loops between the prefrontal cortex, premotor cortex, motor cortex, basal ganglia, and thalamus [11,12] (Fig. 2).

Table 1 Demographic, biomarker, and neuropsychological data of the two groups

|	PMR+	PMR−	Significance, P
Demographic variables			
N (total n = 24)	12	12	
Age, years	69.75 ± 5.96	69.08 ± 7.37	0.932
Age range, years	55–75	59–78	
Sex: % male	41.67	66.67	
Education, years	13.00 ± 2.67[a]	12.82 ± 3.55[b]	0.973
Biomarkers			
Apolipoprotein ε4	0.67 ± 0.65	1.00 ± 0.78[b]	0.347
CSF beta-amyloid (1-42)	539.00 ± 99.87	569.17 ± 105.62	0.590
CSF tau	675.58 ± 253.20	655.33 ± 269.46	0.843
CSF phospho-tau	89.33 ± 41.44	79.91 ± 25.81[b]	0.880
Neuropsychological variables			
Hamilton depression scale	2.80 ± 2.57[a]	2.64 ± 1.69[b]	0.918
Mini-mental status examination	24.45 ± 2.58[b]	25.00 ± 2.86[b]	0.699
DemTect	3.10 ± 0.99[a]	3.09 ± 1.14[b]	0.918
Verbal learning memory test, total learning	27.45 ± 5.36[b]	28.45 ± 6.20[b]	0.847
Verbal learning memory test, delayed recall	2.73 ± 2.15[b]	2.73 ± 2.69[b]	0.797
Logical memory, immediate recall	21.90 ± 6.39[a]	17.73 ± 9.26[b]	0.349
Logical memory, delayed recall	8.30 ± 7.21[a]	7.73 ± 5.90[b]	0.809
Logical memory, recognition	13.80 ± 6.25[a]	15.55 ± 2.91[b]	0.426
Design memory, total learning	44.29 ± 6.50[c]	40.00 ± 8.94[a]	0.364
Design memory, delayed recall	38.86 ± 6.51[c]	38.60 ± 10.01[a]	0.887
Symbol span	11.00 ± 4.15[d]	9.27 ± 3.74[b]	0.331
Digit span	12.30 ± 2.11[a]	13.18 ± 3.13[b]	0.705
Autobiographical memory, long-term memory	3.45 ± 1.04[b]	4.18 ± 1.72[b]	0.217
Autobiographical memory, short-term memory	2.82 ± 0.87[b]	2.64 ± 1.12[b]	0.748
Trail making test: A, s	56.39 ± 14.62[a]	85.19 ± 50.72[b]	0.152
Trail making test: B, s	210.06 ± 77.79[c]	249.72 ± 141.68[a]	0.720
Regensburger word fluency test, professions	11.80 ± 3.08[a]	10.27 ± 3.17[b]	0.314
Regensburger word fluency test, names	17.09 ± 5.54[b]	15.82 ± 3.87[b]	0.401
Regensburger word fluency test, S-words	8.60 ± 4.99[a]	6.40 ± 4.14[a]	0.280
Regensburger word fluency test, K-words	11.30 ± 3.56[a]	8.80 ± 3.29[a]	0.075
Brief test of attention	13.80 ± 3.49[a]	11.40 ± 4.95[a]	0.481
Money road map test	24.57 ± 4.69[c]	28.10 ± 4.84[a]	0.109

CSF, cerebrospinal fluid; PMR+, palmomental reflex-positive group; PMR−, palmomental reflex-negative group. [a]Two missing data sets. [b]One missing data set. [c]Five missing data sets. [d]Three missing data sets.

The details of the neural circuitry underlying the PMR is yet unknown [31]. However, general anatomical and functional connections linking the stimulation of the thenar eminence to the mentalis muscle response have been identified. These are all part of the motor circuit: the ventrolateral thalamus is the site where efferent projections from the basal ganglia terminate. The ventrolateral thalamus sends afferent projections to the area representing the arm in the somatotopically organized SMA [32,33], which in turn is also involved in facial movements [33,34] and provides extensive connections between the somatotopically arranged regions.

Alterations in the structures associated with the interconnecting motor circuit are likely to play a role in the pathogenesis of a reoccurred PMR. Our findings, which demonstrate decreased FC between constituents of the motor circuit, support this hypothesis regarding patients with AD.

Applying a more liberal statistical threshold, the ROI-to-ROI FC analysis revealed a decreased FC between the left putamen and the left SFG in the PMR-positive group (compared to the PMR-negative group). The latter finding corresponds well with a reduced cerebral metabolism between the left SFG and the left putamen observed in a recent study using ^{18}F-fluorodeoxyglucose positron-emission tomography (FDG-PET) in patients with positive primitive reflexes (grasp, palmomental, suck and glabellar reflex) and dementia [11]. Taken together, these findings suggest aberrant frontostriatal connectivity in the pathogenesis of the PMR.

The increased incidence of the PMR in patients with basal ganglia disorders [10,35], as well as the presumed role of frontal lobe dysfunction with reoccurring primitive reflexes [6,36,37], support our hypothesis that the reoccurrence of the PMR in AD is associated with dysfunction of the motor circuitry
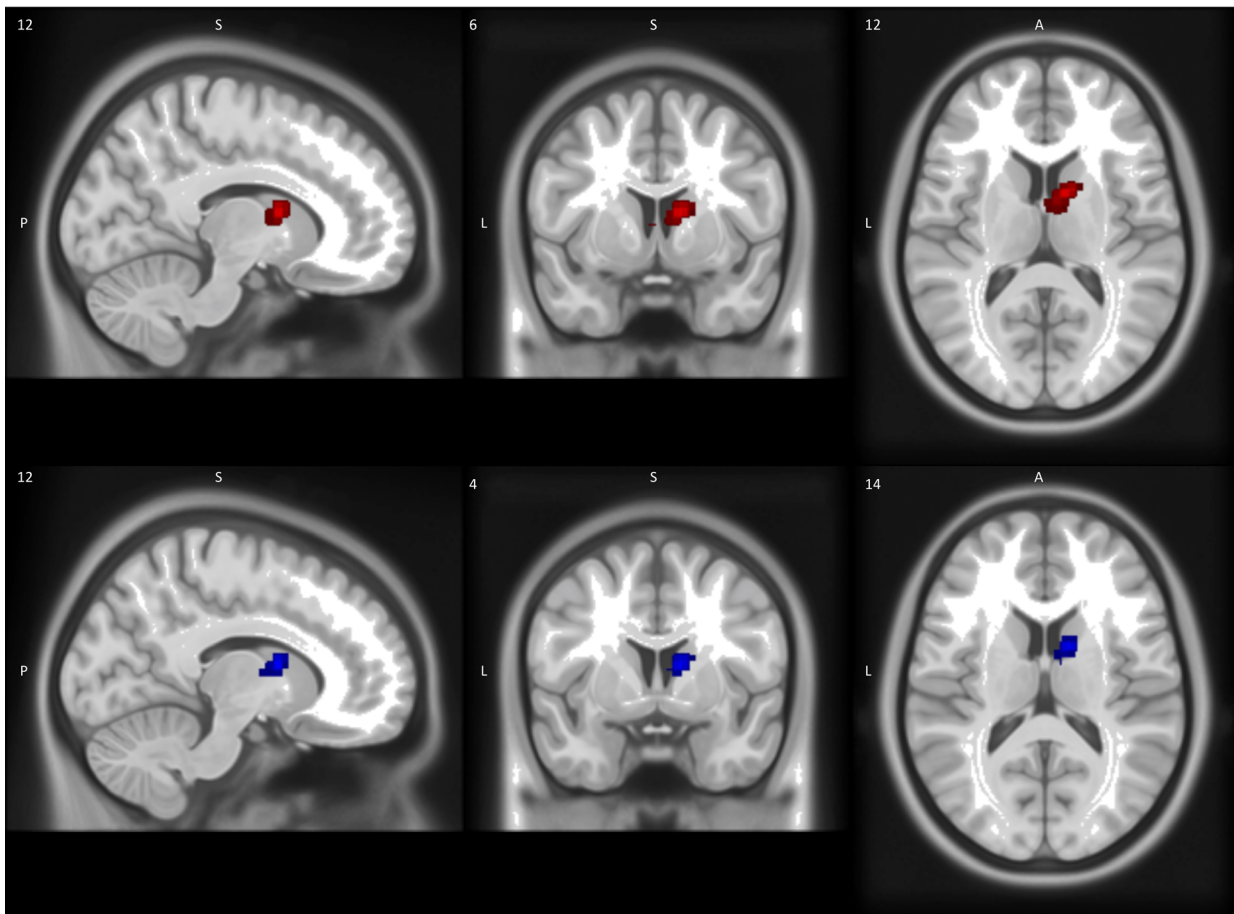
Figure 1 Above: functional connectivity (FC) cluster emerging from the left supplementary motor area (SMA) seed. Below: FC cluster emerging from the right SMA seed. The sagittal, coronal, and transversal perspectives are depicted. Numbers represent Montreal Neurological Institute coordinates; A, anterior; L, left; P, posterior; S, superior. [Colour figure can be viewed at wileyonlinelibrary.com]

Table 2 Seed-to-voxel analysis: reduced functional connectivity in the palmomental reflex (PMR)-positive compared to the PMR-negative group

Seeds	Cluster MNI coordinates			Voxels	Peak-voxel FWE corrected P value	ROIs within the cluster (voxel count)
	x	y	z			
SMA, left	12	6	12	251	0.001	Caudate right (85); thalamus right (42)
SMA, right	12	4	14	185	0.004	Caudate right (72); thalamus right (38)

FWE, family-wise error; MNI, Montreal Neurological Institute; SMA, supplementary motor area.

resulting from aberrant connectivity between the basal ganglia and frontal cortex. As we did not observe significant structural group differences corresponding to the shown aberrant FC, one can assume that the PMR indicates changes in FC before or independent of changes in SC. Such independence is supported by recent studies, postulating that white matter SC is not correlated to the corresponding changes in cortical resting-state FC, at least in normal aging [38] and that FC anomalies can be detected prior to structural changes, suggesting an unsynchronized pace of structural and functional changes [39]. At the same time, compensatory changes in FC could temporarily mask the underlying structural deficiencies (e.g. atrophy) [40]. Even though the interconnecting loops between the basal ganglia and the frontal cortex are also involved in learning, memory and attention [12,41], the two groups of AD patients studied did not differ in their neuropsychological testing performance. This suggests that the aberrant frontostriatal FC in AD

**Table 3** Probabilistic tractography between the two groups

		PMR−		PMR+		
ROI 1	ROI 2	Mean CS	SD	Mean CS	SD	Significance, P
SMA right	CE1 right	0.057	0.042	0.132	0.119	0.250
SMA right	CE2 right	0.067	0.051	0.178	0.151	0.155
SMA right	Caudate right	0.058	0.024	0.057	0.026	0.999
SMA right	Thalamus right	0.083	0.044	0.093	0.042	0.999
SFG left	Putamen left	0.210	0.055	0.204	0.083	0.999

CE1, CONN-exported cluster covering parts of the right caudate nucleus and right thalamus; CE2, CE1 multiplied by an atlas-based mask of the right caudate nucleus; CS, connection strength; PMR+, palmomental reflex-positive group; PMR−, palmomental reflex-negative group; ROI, region of interest; SFG, superior frontal gyrus; SMA, supplementary motor area.

Table 4 Morphometric brain volume differences in palmomental reflex (PMR)-negative > PMR-positive using voxel-based morphometry

	MNI coordinates				
Anatomical structure	x	y	z	Voxels	P (uncorrected)
Superior parietal lobule left	−28	−75	48	25	<0.001
Superior frontal gyrus right	16	58	38	18	<0.001
Middle temporal gyrus left[a]	−30	24	−39	14	0.001

MNI, Montreal Neurological Institute; [a]MNI coordinates represent most likely the left middle temporal gyrus.
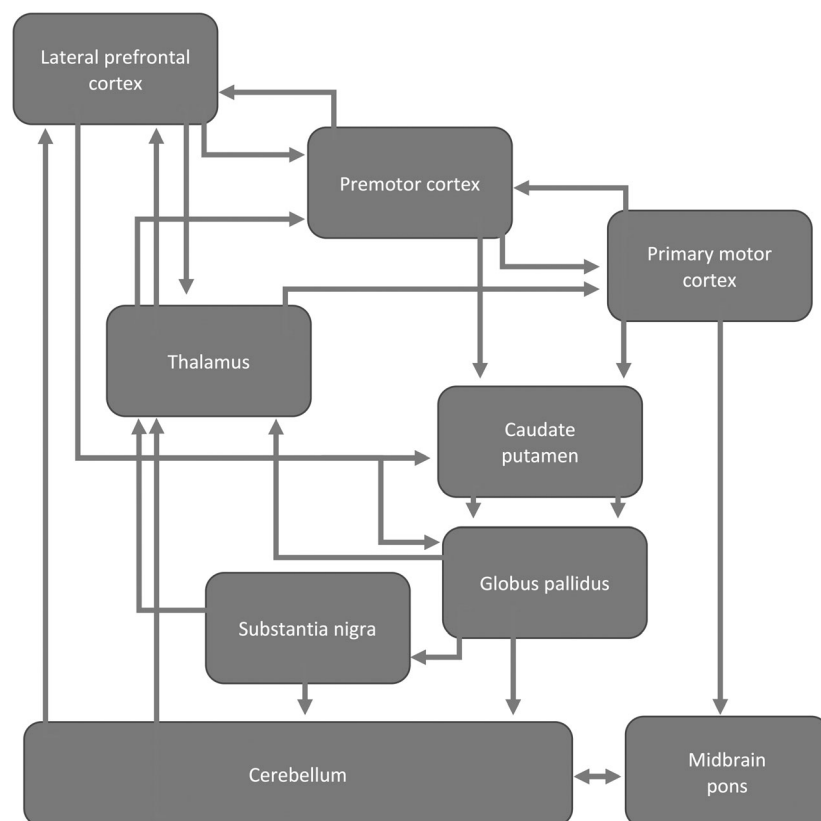
Figure 2 Interconnectivity of the structures being part of the corticostriatal motor circuit (adapted from Fuster 2015, Chapter VI, Page 45).

patients with positive PMR differentially affected the motor circuitry involved in the suppression of primitive reflexes. This hypothesis is consistent with the finding that AD affects different cognitive domains, compared to dementia, associated with a dysfunction of the basal ganglia or the frontal lobe (i.e. Parkinson's disease dementia, frontotemporal dementia) [42]. The differential involvement of the motor circuitry in the different forms of dementia warrants further investigation.

One methodological limitation of performing tractography in patients with AD is the variable atrophy pattern caused by both aging and AD [43]. As a result, the sizes of our seed and target masks varied considerably between subjects. Furthermore, the variability in mask size depended on a cortical or subcortical localization, as brain atrophy is often more distinct in cortical areas. Normalizing connection probabilities to the mask size may be insufficient to account for these effects. In contrast, atrophy-associated effects on resting-state networks seem to be rather limited [44].

Functional connectivity measures were performed using a bivariate correlation method as this has proven to be very suitable for functional MRI FC analyses. However, since there are various methods to calculate the FC and none of them is clearly superior [45], further analyses should try to replicate the results with other FC measures. One further limitation of our study is the somewhat limited sample size. Future studies replicating and extending the present findings are warranted.

In conclusion, data suggest that dysfunction of the CMC reflected by decreased FC underlies a positive PMR in AD. The lack of significant grey matter or SC differences might reflect that changes in FC appear before changes of SC in the structures of the CMC and brain atrophy.

Acknowledgments

Disclosure of conflict of interest

The authors declare no financial or other conflicts of interest.

Data availability statement

The data that support the findings of this study are available from the corresponding author upon reasonable request.

References

1. Fillenbaum GG, van Belle G, Morris JC, *et al*. Consortium to establish a registry for Alzheimer's disease (CERAD): the first twenty years. *Alzheimers Dement* 2008; **4:** 96–109.
2. Pfeffer A, Gabryelewicz T, Barczak A, Èuczywek E, Wasiak B, Bardkowska M. Does the presence of palmomental reflex help predict MCI course? *J Neurol Sci* 2005; **238:** S297.
3. Streit S, Limacher A, Zeller A, Burge M. Detecting dementia in patients with normal neuropsychological screening by short smell test and palmo-mental reflex test: an observational study. *BMC Geriatr* 2015; **15:** 90.
4. Liao KK, Chen JT, Lai KL, *et al*. Brainstem excitability is increased in subjects with palmomental reflex. *J Formos Med Assoc* 2007; **106:** 601–607.
5. Whittle IR, Miller JD. Clinical usefulness of the palmomental reflex. *Med J Aust* 1987; **146:** 137–139.
6. Ladino LD, Isaza S, Delgado J, *et al*. Diagnostic yield of the palmomental reflex in patients with suspected frontal lesion. *J Neurol Sci* 2015; **359:** 156–160.
7. Owen G, Mulley GP. The palmomental reflex: a useful clinical sign? *J Neurol Neurosurg Psychiatry* 2002; **73:** 113–115.
8. Reis DJ. The palmomental reflex. A fragment of a general nociceptive skin reflex: a physiological study in normal man. *Arch Neurol* 1961; **4:** 486–498.
9. Schott JM, Rossor MN. The grasp and other primitive reflexes. *J Neurol Neurosurg Psychiatry* 2003; **74:** 558–560.
10. Marterer-Travniczek A, Danielczyk W, Muller F, Simanyi M, Fischer P. Release signs in Parkinson's disease with and without dementia. *J Neural Transm Park Dis Dement Sect* 1992; **4:** 207–212.
11. Matias-Guiu JA, Cabrera-Martin MN, Fernadez-Matarrubia M, *et al*. Topography of primitive reflexes in dementia: an F-18 fluorodeoxyglucose positron emission tomography study. *Eur J Neurol* 2015; **22:** 1201–1207.
12. Fuster JM. *The prefrontal cortex*. Fifth edition. Amsterdam; Boston: Elsevier/AP, Academic Press is an imprint of Elsevier: 2015.
13. Dillen KN, Jacobs HI, Kukolja J, *et al*. Aberrant functional connectivity differentiates retrosplenial cortex from posterior cingulate cortex in prodromal Alzheimer's disease. *Neurobiol Aging* 2016; **44:** 114–126.
14. Albert MS, DeKosky ST, Dickson D, *et al*. The diagnosis of mild cognitive impairment due to Alzheimer's disease: recommendations from the national institute on aging-Alzheimer's association workgroups on diagnostic guidelines for Alzheimer's disease. *Alzheimers Dement* 2011; **7:** 270–279.
15. Jack CR Jr, Bennett DA, Blennow K, *et al*. A/T/N: an unbiased descriptive classification scheme for Alzheimer disease biomarkers. *Neurology* 2016; **87:** 539–547.
16. Mulder C, Verwey NA, van der Flier WM, *et al*. Amyloid-beta(1–42), total tau, and phosphorylated tau as

cerebrospinal fluid biomarkers for the diagnosis of Alzheimer disease. *Clin Chem* 2010; **56:** 248–253.

17. Dillen KNH, Jacobs HIL, Kukolja J, *et al*. Functional disintegration of the default mode network in prodromal Alzheimer's disease. *J Alzheimers Dis* 2017; **59:** 169–187.

18. Whitfield-Gabrieli S, Nieto-Castanon A. Conn: a functional connectivity toolbox for correlated and anticorrelated brain networks. *Brain Connect* 2012; **2:** 125–141.

19. Desikan RS, Segonne F, Fischl B, *et al*. An automated labeling system for subdividing the human cerebral cortex on MRI scans into gyral based regions of interest. *NeuroImage* 2006; **31:** 968–980.

20. Woolrich MW, Jbabdi S, Patenaude B, *et al*. Bayesian analysis of neuroimaging data in FSL. *NeuroImage* 2009; **45:** S173–S186.

21. Li X, Morgan PS, Ashburner J, Smith J, Rorden C. The first step for neuroimaging data analysis: DICOM to NIfTI conversion. *J Neurosci Methods* 2016; **264:** 47–56.

22. Smith SM. Fast robust automated brain extraction. *Hum Brain Mapp* 2002; **17:** 143–155.

23. Jenkinson M, Bannister P, Brady M, Smith S. Improved optimization for the robust and accurate linear registration and motion correction of brain images. *NeuroImage* 2002; **17:** 825–841.

24. Maldjian JA, Laurienti PJ, Kraft RA, Burdette JH. An automated method for neuroanatomic and cytoarchitectonic atlas-based interrogation of fMRI data sets. *NeuroImage* 2003; **19:** 1233–1239.

25. Tzourio-Mazoyer N, Landeau B, Papathanassiou D, *et al*. Automated anatomical labeling of activations in SPM using a macroscopic anatomical parcellation of the MNI MRI single-subject brain. *NeuroImage* 2002; **15:** 273–289.

26. Andersson JL, Sotiropoulos SN. An integrated approach to correction for off-resonance effects and subject movement in diffusion MR imaging. *NeuroImage* 2016; **125:** 1063–1078.

27. Jbabdi S, Sotiropoulos SN, Savio AM, Grana M, Behrens TE. Model-based analysis of multishell diffusion MR data for tractography: how to get over fitting problems. *Magn Reson Med* 2012; **68:** 1846–1855.

28. Behrens TE, Woolrich MW, Jenkinson M, *et al*. Characterization and propagation of uncertainty in diffusion-weighted MR imaging. *Magn Reson Med* 2003; **50:** 1077–1088.

29. Pelzer EA, Melzer C, Timmermann L, von Cramon DY, Tittgemeyer M. Basal ganglia and cerebellar interconnectivity within the human thalamus. *Brain Struct Funct* 2017; **222:** 381–392.

30. Ashburner J. A fast diffeomorphic image registration algorithm. *NeuroImage* 2007; **38:** 95–113.

31. Mills KR. *Oxford textbook of clinical neurophysiology*. Oxford: Oxford University Press; 2016.

32. Dum RP, Strick PL. The origin of corticospinal projections from the premotor areas in the frontal lobe. *J Neurosci* 1991; **11:** 667–689.

33. Fried I, Katz A, McCarthy G, *et al*. Functional organization of human supplementary motor cortex studied by electrical stimulation. *J Neurosci* 1991; **11:** 3656–3666.

34. Cattaneo L, Pavesi G. The facial motor system. *Neurosci Biobehav Rev* 2014; **38:** 135–159.

35. Jensen JP, Gron U, Pakkenberg H. Comparison of three primitive reflexes in neurological patients and in normal individuals. *J Neurol Neurosurg Psychiatry* 1983; **46:** 162–167.

36. Bracha S. The clinical value of the pollico-mental reflex in neuropathology. *J Nerv Ment Dis* 1958; **127:** 91–94.

37. Whittle IR, Miller JD. The palmomental reflex. *Surg Neurol* 1986; **26:** 521.

38. Tsang A, Lebel CA, Bray SL, *et al*. White matter structural connectivity is not correlated to cortical resting-state functional connectivity over the healthy adult lifespan. *Front Aging Neurosci* 2017; **9:** 144.

39. Zhao J, Du YH, Ding XT, Wang XH, Men GZ. Alteration of functional connectivity in patients with Alzheimer's disease revealed by resting-state functional magnetic resonance imaging. *Neural Regen Res* 2020; **15:** 285–292.

40. Cabeza R, Albert M, Belleville S, *et al*. Maintenance, reserve and compensation: the cognitive neuroscience of healthy ageing. *Nat Rev Neurosci* 2018; **19:** 701–710.

41. Leisman G, Braun-Benjamin O, Melillo R. Cognitive-motor interactions of the basal ganglia in development. *Front Syst Neurosci* 2014; **8:** 16.

42. Stout JC, Johnson SA. Cognitive impairment and dementia in basal ganglia disorders. *Curr Neurol Neurosci Rep* 2005; **5:** 355–363.

43. Stepan-Buksakowska I, Szabo N, Horinek D, *et al*. Cortical and subcortical atrophy in Alzheimer disease: parallel atrophy of thalamus and hippocampus. *Alzheimer Dis Assoc Disord* 2014; **28:** 65–72.

44. Conwell K, von Reutern B, Richter N, Kukolja J, Fink GR, Onur OA. Test-retest variability of resting-state networks in healthy aging and prodromal Alzheimer's disease. *Neuroimage Clin* 2018; **19:** 948–962.

45. Wang HE, Benar CG, Quilichini PP, Friston KJ, Jirsa VK, Bernard C. A systematic framework for functional connectivity measures. *Front Neurosci* 2014; **8:** 405.

THE IMPORTANCE OF GREY AND WHITE MATTER

In Multiple Sclerosis

Visit GreyAndWhiteMS.com for more information.